Soft Matter

Side-Chain Halogen Effects on Self-Assembly and Hydrogelation of Cationic Phenylalanine Derivatives

Journal:	*Soft Matter*
Manuscript ID	SM-ART-05-2022-000713.R1
Article Type:	Paper
Date Submitted by the Author:	16-Jul-2022
Complete List of Authors:	Abraham, Brittany; University of Rochester, Chemistry Mensah, Samantha; University of Rochester, Chemistry; Gwinnell, Benjamin; University of Rochester Nilsson, Bradley; University of Rochester, Chemistry

Side-Chain Halogen Effects on Self-Assembly and Hydrogelation of Cationic Phenylalanine Derivatives

*Brittany L. Abraham,[a] Samantha G. Mensah,[a] Benjamin R. Gwinnell,[a] and Bradley L. Nilsson[a,b]**

[a]Department of Chemistry, University of Rochester, Rochester, NY 14627, USA.

[b]Materials Science Program, University of Rochester, Rochester, NY 14627, USA.

E-mail: bradley.nilsson@rochester.edu

Fax: +1 585 276-0205; Tel. +1 585 276-3053

Abstract

Low molecular weight (LMW) supramolecular hydrogels have great potential as next-generation biomaterials for drug delivery, tissue engineering, and regenerative medicine. The design of LMW gelators is complicated by the lack of understanding regarding how the chemical structure of the gelator correlates to self-assembly potential and emergent hydrogel material properties. The fluorenylmethyloxycarbonyl-phenylalanine (Fmoc-Phe) motif is a privileged scaffold that is prone to undergo self-assembly into self-supporting hydrogel networks. Cationic Fmoc-Phe-DAP derivatives modified with diaminopropane (DAP) at the C-terminus have been developed that self-assemble into hydrogel networks in aqueous solutions of sufficient ionic strength. We report herein the impact of side-chain halogenation on the self-assembly and hydrogelation properties of Fmoc-Phe-DAP derivatives. A systematic study of the self-assembly and hydrogelation of monohalogenated Fmoc-Phe-DAP derivatives with F, Cl, or Br atoms in the *ortho*, *meta*, or *para* positions of the phenyl side chain reveal significant differences in self-assembly and gelation potential, nanoscale assembly morphology, and hydrogel viscoelastic properties as a function of halogen identity and substitution position. These results demonstrate the profound impact that subtle changes to the chemical scaffold can have on the behavior of LMW supramolecular gelators and illustrate the ongoing difficulty of predicting the emergent self-assembly and hydrogelation behavior of LMW gelators that differ even modestly in chemical structure.

Introduction

Supramolecular hydrogels are promising next-generation materials for drug delivery, tissue engineering, and regenerative medicine.[1-3] Hydrogels composed of self-assembled macromolecules such as peptides have been developed that exhibit the ideal physical and biochemical properties for the aforementioned biomedical applications.[4-9] However, the high cost of the constituent peptides has been an impediment to the widespread adoption of these hydrogels as materials for clinical applications.[10-12] Low molecular weight (LMW) supramolecular hydrogels have emerged as cost-effective alternatives to peptide-based materials.[13-17] However, the development of LMW hydrogels that possess the complete range of emergent properties shown by supramolecular peptide hydrogels has been challenging.[17-19] It has proven difficult to accurately predict the emergent self-assembly and viscoelastic character of LMW gelators as a function of the chemical structure of the gelator.[20-21] This is due, in part, to a lack of understanding regarding how the molecular packing structure of the self-assembled material is related to the properties of the gelator.[22]

Phenylalanine (Phe) derivatives are a privileged class of LMW supramolecular gelator due to their propensity to undergo noncovalent self-assembly.[23-25] We and others have found that Phe-derived supramolecular hydrogels have viscoelastic properties that approach those of peptide-based gels.[26-36] The self-assembly and gelation of Phe derivatives is highly sensitive to even modest changes in chemical structure.[36-44] For example, we have found that side-chain halogenation of fluorenylmethyloxycarbonyl-phenylalanine (Fmoc-Phe) scaffolds imparts enhanced gelation capacity to these derivatives compared to the parent Fmoc-Phe molecule, with pentafluorination of the side chain (Fmoc-F_5-Phe) leading to hydrogels with superior emergent properties.[45] The self-assembly rate and resulting hydrogel viscoelasticity of monohalogenated

Fmoc-Phe derivatives was also found to be highly sensitive to both the side-chain halogen identity and halogenation pattern.[46] Halogenation position on the phenyl ring determined the rate of assembly, increasing in the order *ortho* < *meta* < *para*. Hydrogel rigidity trended with both halogen position and identity, increasing in the order *para* < *ortho* < *meta* for each halogen and in the order Br < Cl < F within each substitution pattern group. Thus, though a similar fibrillar morphology was observed for all derivatives, the emergent properties of the resulting hydrogels proved to be quite sensitive to single-atom variations in the chemical structure.

In addition to side-chain modification, we have also reported cationic Fmoc-Phe derivatives modified at the C-terminus that self-assemble into fibrillar or nanotube hydrogel networks (**Figure 1**).[47] The cationic Fmoc-Phe-DAP class of gelators undergo self-assembly upon addition of physiologically relevant concentrations of sodium chloride, which acts to promote self-assembly by screening repulsive charge-charge interactions. As with the parent Fmoc-Phe derivatives, the cationic Fmoc-F_5-Phe-DAP and Fmoc-3F-Phe-DAP form hydrogels with higher viscoelasticity compared to Fmoc-Phe-DAP (**Figure 1A**).[47-48] However, while Fmoc-Phe and its fluorinated variants exhibit a similar fibrillar morphology upon gelation in all cases, the morphologies observed from assembled Fmoc-Phe-DAP derivatives are more varied and complex. Fmoc-Phe-DAP self-assembles into fibrils that further hierarchically assemble into flat nanoribbons, which finally roll into nanotubes over a period of days. Fmoc-3F-Phe-DAP follows a similar assembly progression but requires a longer sample aging time or a higher temperature to favor formation of the nanoribbons and nanotubes. In contrast, Fmoc-F_5-Phe-DAP lacks the same hierarchical assembly pattern, instead forming opaque hydrogels composed of fibers that are apparently unaffected by progression of time and changes in temperature.

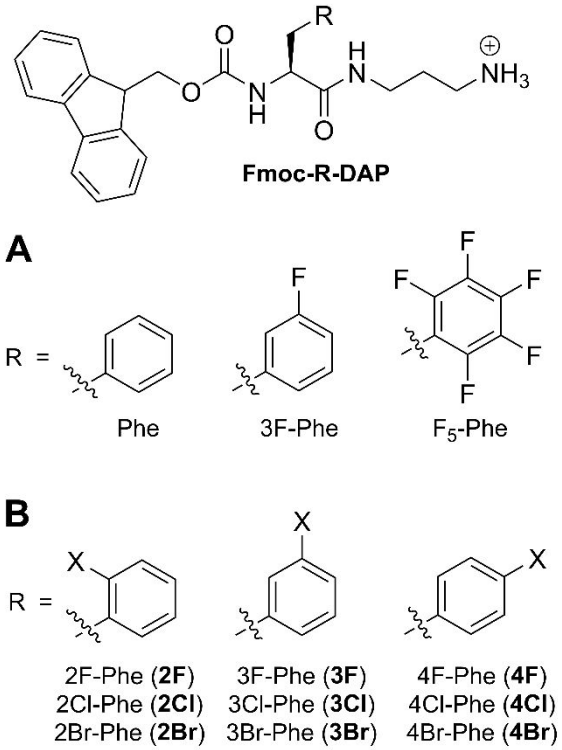

Figure 1. Chemical structures of Fmoc-Phe-DAP derivatives. (A) Fmoc-Phe-DAP, Fmoc-3F-Phe-DAP, and Fmoc-F_5-Phe-DAP gelators. (B) Fmoc-2X-Phe-DAP, Fmoc-3X-Phe-DAP, and Fmoc-4X-Phe-DAP gelators, where X = F, Cl, or Br.

Based on our previous observations of Fmoc-X-Phe gelator behavior, we hypothesized that self-assembly and gelation of Fmoc-Phe-DAP derivatives might be similarly sensitive to side-chain halogenation patterns. Accordingly, we herein report the effects of both halogen identity (F, Cl, or Br) and ring position (*ortho*, *meta*, or *para*) on the self-assembly of monohalogenated Fmoc-X-Phe-DAP derivatives (**Figure 1B**). As with Fmoc-X-Phe gelators, the position and identity of halogens in Fmoc-X-Phe-DAP derivatives had a significant effect on the morphology and viscoelasticity of resultant hydrogels. Nanostructure morphology varied across the samples, with halogen position dictating the type of nanostructure formed in the *ortho*- and *meta*-substituted gelator groups and halogen identity having a strong impact in the *para* substitution position. Trends

in viscoelastic properties of the assemblies were not as clear due to substantial differences in assembly morphology, although the *ortho*-substituted derivatives generally formed hydrogels with the weakest viscoelastic moduli. Overall, single-halogen variations in identity and position prove to exert a significant effect on the self-assembly and hydrogelation of LMW Fmoc-Phe-DAP gelators, granting access to materials with a range of emergent properties. These results illustrate the unpredictability of the effects of subtle modifications of chemical structure on the emergent properties of the resultant hydrogels. This work underscores the need for additional insight into the correlation between chemical structure, supramolecular self-assembly, and the emergent properties of the assembled networks.

Experimental

Materials. Reagents and organic solvents were purchased commercially and used without further purification. All compounds (**Figure 1B**: **2X**, **3X**, **4X**, X = F, Cl, Br) were synthesized by a modified version of the previously reported protocol.[49] Detailed synthetic protocols and characterization data for the new compounds are reported in the Electronic Supplementary Information (ESI). Water used for gelation was purified using a nanopure filtration system (Barnstead NANOpure, 0.2 μm filter, 18 Ω).

NMR Spectroscopy. NMR spectra were obtained using Brüker Avance 400 and 500 MHz spectrometers. ^{1}H, ^{13}C, and ^{19}F chemical shifts are reported as δ with reference to TMS at 0 ppm for ^{1}H, residual solvent for ^{13}C, and $CFCl_3$ at 0 ppm for ^{19}F NMR. See the ESI for NMR spectra and tabulated data of all compounds except **3F**, which was previously reported.[47]

Mass Spectrometry. High-resolution mass spectra were acquired on a Thermo Fisher Q Exactive™ Plus Hybrid Quadrupole-Orbitrap™ Mass Spectrometer in positive mode. See the ESI for mass spectra and tabulated data.

Self-Assembly Conditions. All compounds were assembled with a final gelator concentration of 10 mM, final NaCl concentration of 114 mM, and total volume of 2 mL. Compounds **2X–4X** (0.02 mmol) were dissolved in 1.6 mL of nanopure water in a glass vial by heating the vial in a 70 ºC water bath for 60 seconds, followed by sonication for 30 seconds, followed by heating again for an additional 30 seconds. Then, 0.4 mL of a 570 mM aqueous NaCl solution was added to the vial, which was immediately and briefly agitated by vortex mixer. The samples were allowed to stand for 30 minutes, then the vial was inverted to determine if the sample was a self-supporting hydrogel or a viscous colloidal suspension.

Transmission Electron Microscopy (TEM). TEM images were obtained using a Hitachi 7650 transmission electron microscope with an accelerating voltage of 80 kV. Each sample (8 μL) was applied directly onto 200 mesh carbon-coated copper grids and allowed to stand for 1 minute. Excess sample was removed carefully by capillary action using filter paper. Each grid was then stained with 2% (w/v) uranyl acetate solution (8 μL) for 2 minutes, and excess stain was removed via capillary action using filter paper. Grids were allowed to air dry for at least 10 minutes. Dimensions of nanostructures were determined using ImageJ software and are reported as the average of at least 100 independent measurements with error reported as the standard deviation about the mean, or as a range for nanotubes that occurred infrequently or that varied widely in size.

Oscillatory Rheology. Rheological measurements were obtained using a TA Instruments Discovery HR-2 rheometer operating in oscillatory mode. A 20 mM parallel plate geometry and standard Peltier plate were used for the experiments. Hydrogels of 1 mL volume were formed in

1.5 mL plastic microcentrifuge tubes following the standard assembly procedure discussed above and allowed to stand for 24 hours. Immediately prior to rheological characterization, the plastic tube containing the hydrogel was cut at the 0.5 mL line using a razor blade and the cylindrical hydrogel from the top portion of the tube was placed directly onto the Peltier plate for characterization. Experiments were performed with an average gap size of 1.2 mm. To determine the linear viscoelastic region for each sample, strain sweeps were performed from 0.01%–100% strain at a constant angular frequency of 6.283 rad s^{-1}. All strain sweeps are provided in the ESI (**Figure S30**). Frequency sweeps for each sample were performed from 0.1–100 rad s^{-1} at a constant strain of 0.2%, which was within the linear viscoelastic region for all hydrogels studied. Immediately prior to each frequency sweep, a time sweep at constant strain of 0.2% and constant angular frequency of 0.1 rad s^{-1} was performed for 5 minutes to allow the sample to equilibrate on the plate after the transfer process. Values at the upper end of the frequency sweep were cut off from reported data when the raw phase angle increased above 175º as recommended for the TA DHR series of rheometers, since values beyond this point are dominated by the instrument inertial torque instead of the sample torque (most prominently seen in samples with low G′/G″ values).[50] Reported values for storage and loss moduli (G′ and G″, respectively) are the average of at least three distinct measurements on separate hydrogels with the error reported as the standard deviation about the mean. All frequency sweeps are provided in the ESI (**Figure S31**).

Results and Discussion

Self-Assembly and Hydrogelation of Fmoc-X-Phe-DAP Derivatives. The gelation capacity of Fmoc-X-Phe-DAP compounds **2X–4X** (**Figure 1**) was assessed by mixing a solution of each gelator with sodium chloride to increase the ionic strength and initiate self-assembly. Each gelator

was dissolved in water by heating and sonication of the vial, then an aliquot of aqueous sodium chloride was added, and the vial was briefly agitated by vortex mixer. Samples were assembled at a final concentration of 10 mM gelator and 114 mM sodium chloride. After 30 minutes had elapsed, each vial was inverted to check for the formation of a self-supporting hydrogel (**Figure 2**). Of the *ortho*-substituted derivatives, **2F** and **2Cl** formed viscous, slightly turbid colloidal suspensions that did not withstand vial inversion, while **2Br** formed a slightly turbid hydrogel (**Figure 2A–C**). In contrast, all *meta*-substituted derivatives, **3F**, **3Cl**, and **3Br**, formed self-supporting hydrogels with varying turbidity, with **3F** forming a transparent hydrogel while hydrogels of **3Cl** and **3Br** were more turbid (**Figure 2D–F**). The *para*-substituted derivatives exhibited the most diverse gelation outcomes; **4F** formed a transparent, self-supporting hydrogel, **4Cl** formed an opaque, weak partial hydrogel, and **4Br** formed a slightly turbid hydrogel (**Figure 2G–I**). Examining the data by halogen identity, it is notable that fluorinated assembles were the most optically transparent regardless of the ring position. This is likely due to the lower hydrophobicity of the fluorinated compounds compared to the others, which was approximated by observing lower retention times upon reverse-phase HPLC analysis under identical mobile and stationary phase conditions (**Figure S27**). However, hydrophobicity alone does not fully account for the observed turbidities. For example, **3Br** was the least optically transparent sample observed but not the most hydrophobic based on the HPLC approximation. Thus, we next examined the assembly morphology of each of these samples on the nanoscale to better understand their emergent properties.

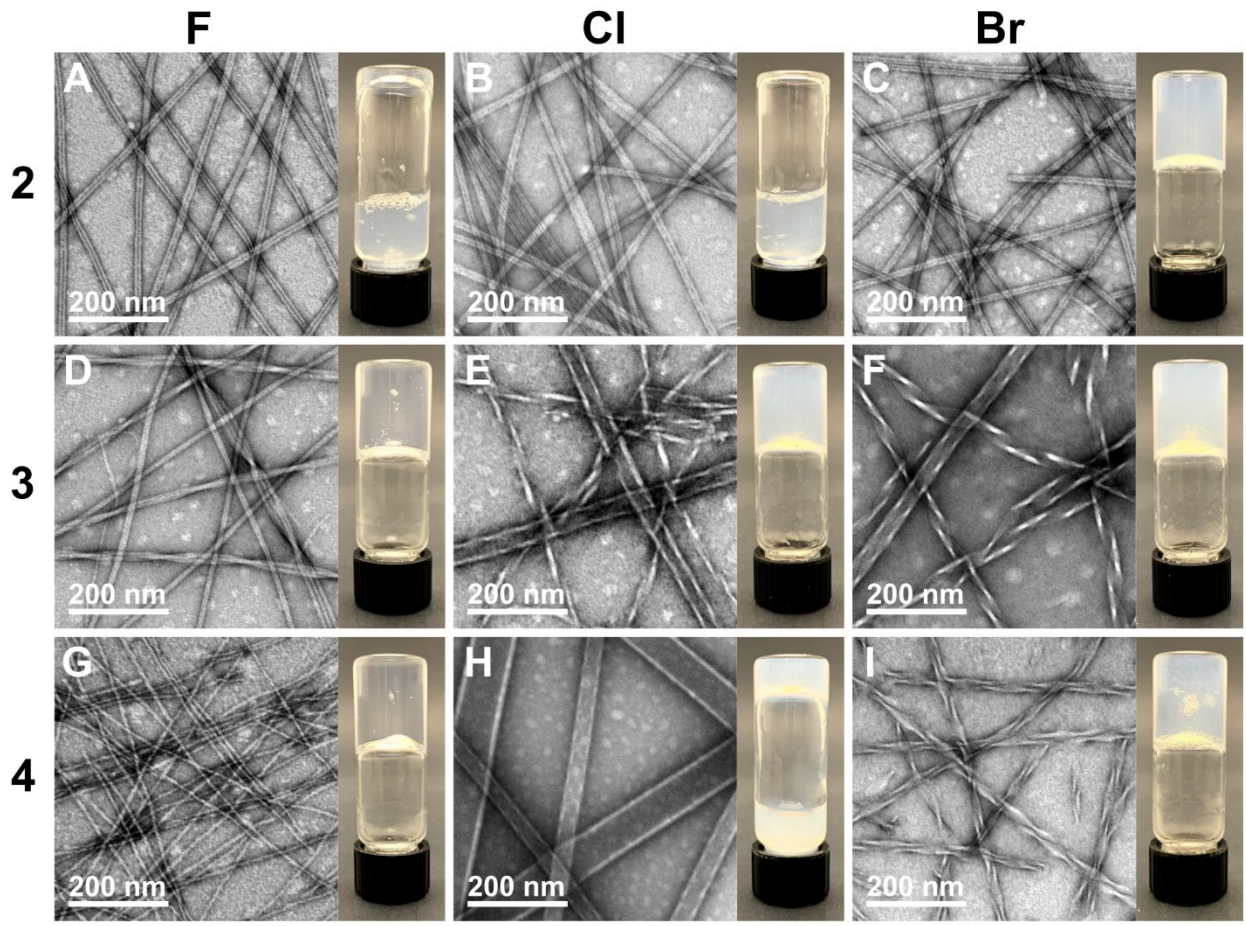

Figure 2. TEM images and digital images of assemblies of compounds **2X–4X** taken 30 minutes after mixing the gelator solution with sodium chloride to initiate self-assembly. (A) Fmoc-2F-Phe-DAP (**2F**); (B) Fmoc-2Cl-Phe-DAP (**2Cl**); (C) Fmoc-2Br-Phe-DAP (**2Br**); (D) Fmoc-3F-Phe-DAP (**3F**); (E) Fmoc-3Cl-Phe-DAP (**3Cl**); (F) Fmoc-3Br-Phe-DAP (**3Br**); (G) Fmoc-4F-Phe-DAP (**4F**); (H) Fmoc-4Cl-Phe-DAP (**4Cl**); (I) Fmoc-4Br-Phe-DAP (**4Br**).

Morphology of Fmoc-X-Phe-DAP Assemblies by TEM. Since we have previously shown that Fmoc-Phe-DAP derivatives assemble into a variety of polymorphic structures, including fibrils, nanoribbons, and nanotubes,[47] we next characterized the effect of halogen identity and ring position on the resulting assembly morphology. All *ortho*-substituted Fmoc-2X-Phe-DAP

derivatives, **2F**, **2Cl**, and **2Br**, assembled into thin nanotubes approximately 15 nm in diameter (**Figure 2A–C**, **Table 1**). Despite the uniform morphological features, these samples exhibited different gelation capacity, indicating that specific halogen-related interactions could be stabilizing the overall network in the case of bromine. Samples were observed up to a week after the initial assembly, and though no morphological changes were observed during this time, the solution of **2Cl** did form a self-supporting hydrogel network that was stable to vial inversion after approximately 24 hours (**Figure S28A–C**). Thus, electronic or steric effects may also contribute to the overall hydrogel stability for the *ortho*-substituted derivatives, since hydrogel stability increases with the halogen identity from F < Cl < Br.

Table 1. Morphology and width of nanostructures observed in samples of gelators **2X–4X** after assembly with sodium chloride. *Note: Single fibril width is provided for **3F**, but the dominant morphology was twisted bundles of 2–3 fibrils.

Gelator	Morphology	Width (nm)
2F	Thin nanotubes	15.3 ± 1.1
2Cl	Thin nanotubes	15.1 ± 1.4
2Br	Thin nanotubes	15.3 ± 1.1
3F	Fibrils*	10.8 ± 0.8
3Cl	Nanoribbons Small nanotubes	38.3 ± 9.2 32.2–50.4
3Br	Nanoribbons Small nanotubes	32.5 ± 4.8 35.0–39.5
4F	Fibrils	6.8 ± 0.6
4Cl	Small nanotubes Large nanotubes	39.2 ± 4.1 92.0 ± 13.6
4Br	Wavy twisted nanoribbons	20.4 ± 1.5

Twisted fibril, nanoribbon, and nanotube assemblies were observed for each of the Fmoc-3X-Phe-DAP derivatives (**Figure 2D–F**). Unlike the *ortho*-substituted derivatives in which each

halogen derivative assembled into similar nanotubes, each of the *meta*-substituted halogen substituent formed unique polymorphic assemblies. Fluorinated **3F** assemblies were twisted bundles of fibrils as previously reported;[49] bundles of 2–3 fibrils were most commonly observed with an individual fibril width of 10.8 ± 0.8 nm (**Table 1**). Chlorinated and brominated derivatives **3Cl** and **3Br** formed similar twisted nanoribbons that were 38.3 ± 9.2 nm and 32.5 ± 4.8 nm wide, respectively (**Table 1**). In each **3Cl** and **3Br** sample, polymorphic nanotubes 30–50 nm in diameter were also observed, apparently formed by the twisted ribbons in which the edges had fused (**Table 1**). The appearance of the larger nanoribbon and nanotube structures generally correlated with an increase in sample turbidity, most likely due to increased light scattering from these assemblies. Additionally, assemblies in hydrogels of **3Cl** and **3Br** exhibited noticeable changes in morphology after aging for one week (**Figure S28E** and **S28F**). We have previously reported that the parent compound, Fmoc-Phe-DAP, undergoes a hierarchical evolution from fibrils to nanoribbons to nanotubes over a period of days.[49] Also as previously reported, this transition is much less pronounced with **3F** when using NaCl to initiate assembly, with nanoribbons and nanotubes only becoming prominent morphologies at high temperatures or over long time periods.[49] In this work, assemblies of **3F** remained unchanged as twisted fibril bundles when allowed to stand at room temperature for one week. Hydrogels of **3Cl** and **3Br** exhibited more extensive nanotube formation after one week than was observed on the first day, a hallmark of the hierarchical progression of assembly structure observed with Fmoc-Phe-DAP. The different morphologies of **3F** fibrils compared to **3Cl** and **3Br** nanoribbons and nanotubes may possibly be due to differences in the steric profile of the appended halogens, with Cl and Br occupying significantly greater volume than F. In addition, the inherent asymmetric electronic distribution of the *meta*-substituted phenyl

ring may also impact assembly morphology of these derivatives, with F being significantly more inductively electron-withdrawing than Cl or Br.

Halogen substitution at the *para* position on the phenyl ring resulted in the largest observed variation in assembly morphology between these derivatives (**Figure 2G–I**). Fluorinated **4F** self-assembled to form thin fibrils that were 6.8 ± 0.6 nm wide. The narrow fibrils dimensions of **4F** assemblies likely explain the high transparency of **4F** hydrogels due to less light scattering (**Figure 2G** and **Table 1**). In striking contrast, the opaque partial hydrogel formed by self-assembly of chlorinated **4Cl** was composed of two groups of nanotubes of smaller and larger diameter (**Figure 2H**). The smaller nanotubes were 39.2 ± 4.1 nm wide, while the larger nanotubes had an average width of 92.0 ± 13.6 nm (**Table 1, Figure S29**). Nanoribbon structures were very rarely observed when examining **4Cl** assemblies, indicating that the nanotubes formed quickly as the dominant, stable morphology. Finally, the brominated **4Br** derivative self-assembled to form wavy twisted nanoribbons with an average width of 20.4 ± 1.5 nm (**Figure 2I** and **Table 1**). The larger size of the nanostructures that define the **4Cl** and **4Br** hydrogels account for their relatively high turbidity, since larger nanostructures will scatter light to a greater degree. No significant changes were observed in these assemblies after observation for 1 week (**Figure S28G–I**). It is fascinating that halogen identity exerts a strong effect on the morphology of assemblies in the *meta* and *para* positions, while the morphology of the *ortho*-substituted assemblies is evidently insensitive to halogen identity. It is possible that the *ortho*-substituents strongly restrict the rotational flexibility of the phenyl ring due to steric interactions and that this restricted rotation defines the assembly morphologies that are accessible. In contrast, this steric effect may be mitigated as the halogen is moved further away from the benzyl carbon, providing a wider range of rotational conformations

of the phenyl ring and amplifying the electronic, hydrophobic, and steric properties of the halogen substituents in the *meta* and *para* substituted derivatives.

Viscoelastic Properties of Fmoc-X-Phe-DAP Assemblies. Hydrogels of Fmoc-X-Phe-DAP derivatives were characterized using oscillatory rheology to interrogate the effects of side-chain halogenation pattern on emergent viscoelastic properties. A strain sweep was performed on each sample at constant angular frequency to determine the linear viscoelastic range for each hydrogel (**Figure S30**). Subsequently, frequency sweep analyses of each sample were performed at a constant strain of 0.2%, which was found to be within the linear viscoelastic range for all hydrogels (**Figure 3**). Average values for the storage (G′) and loss (G″) moduli of each sample were determined from triplicate frequency sweep experiments for each hydrogel (**Table 2** and **Figure S31**). Generally, it was found that G′ and G″ were parallel and nearly independent of frequency, and that G′ exceeded G″ by an order of magnitude, indicating the presence of a structurally robust gel state for all samples.[51] It should be noted that even though compounds **2F**, **2Cl**, and **4Cl** did not form self-supporting hydrogels stable to vial inversion (**Figure 2A**, **2B**, and **2H**), they still possess the viscoelastic characteristics that define a gel state. These three samples had storage moduli under 100 Pa, which did not provide enough elastic or solid-like character for the materials to withstand inversion in glass vials, but these samples can still be considered very weak or soft hydrogels (**Table 2**).

The data were first plotted in groups based on substitution position, since this was the factor that primarily influenced the morphology of self-assembled Fmoc-X-Phe-DAP derivatives (**Figure 3A–C**). *Ortho*-substituted compounds **2F**, **2Cl**, and **2Br**, produced the weakest hydrogels regardless of halogen identity, with storage moduli of 21 ± 2 Pa, 42 ± 3 Pa, and 305 ± 31 Pa,

respectively (**Figure 3A** and **Table 2**). As stated previously, these three samples were composed of nearly identical thin nanotubes, so the presence of bromine specifically in compound **2Br** may be imparting increased stability to the overall network since its viscoelastic moduli are an order of magnitude larger than networks of **2F** and **2Cl**. Interestingly, *meta* substitution of the phenyl ring with fluorine (**3F**) and chlorine (**3Cl**) produced hydrogels with similar G′ values of 1287 ± 51 Pa and 1366 ± 4 Pa, respectively, while hydrogels of the *meta*-brominated derivative **3Br** had a G′ value of only 363 ± 48 Pa (**Figure 3B** and **Table 2**). This is perhaps unexpected since bromination at the *ortho* position resulted in samples with the highest moduli of **2F**, **2Cl**, and **2Br**, but bromination at the *meta* position had the opposite effect, producing hydrogels with moduli that were over three times lower than those of hydrogels of **3F** and **3Cl**. Additionally, hydrogels of **3Cl** and **3Br** showed this variation in viscoelastic moduli despite exhibiting very similar morphologies, indicating again that morphology is not the sole factor influencing the viscoelastic properties of Fmoc-X-Phe-DAP derivatives. Finally, the *para*-substituted derivatives, **4F**, **4Cl**, and **4Br**, formed hydrogels with varying network strength, with G′ values of 1289 ± 110 Pa, 78 ± 4 Pa, and 573 ± 81 Pa, respectively (**Figure 3C** and **Table 2**). The low moduli of hydrogels of **4Cl** could be attributed to the presence of large nanotubes, as we have previously observed that the formation of large nanotubes can destabilize the hydrogel network of the unsubstituted parent molecule, Fmoc-Phe-DAP. No clear overall trend emerged in these viscoelastic data based on halogen position on the phenyl side chain except that *ortho* substitution led to the lowest moduli values.

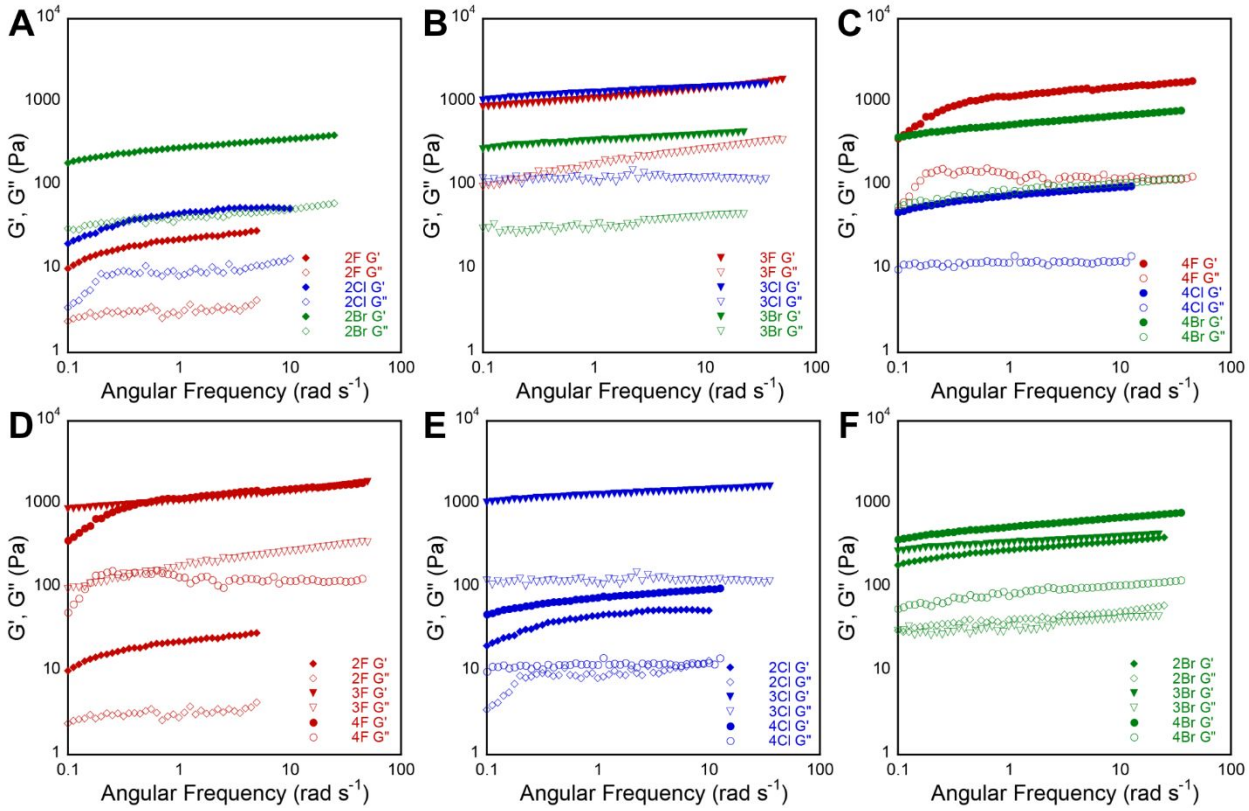

Figure 3. Representative frequency sweep data collected via oscillatory rheology for 10 mM hydrogels of Fmoc-X-Phe-DAP derivatives. G′ and G″ values (Pa) are represented by closed shapes and open shapes, respectively. Fluorinated gelators are graphed in red, chlorinated gelators are graphed in blue, and brominated gelators are graphed in green. *Ortho*-substituted gelators are represented as diamonds, *meta*-substituted gelators are represented as triangles, and *para*-substituted gelators are represented as circles. Values at the upper end of the frequency sweep were cut off from reported data when the raw phase angle increased above 175º as recommended for the TA DHR series of rheometers, since values beyond this point are dominated by the instrument inertial torque instead of the sample torque (most prominently seen in samples with low G′/G″ values).[50] (A–C) Frequency sweeps plotted in groups sorted by substitution position: (A) Fmoc-2X-Phe-DAP derivatives (**2F**, **2Cl**, **2Br**); (B) Fmoc-3X-Phe-DAP derivatives (**3F**, **3Cl**, **3Br**); (C) Fmoc-4X-Phe-DAP derivatives (**4F**, **4Cl**, **4Br**). (D–F) Frequency sweeps plotted in groups sorted

by halogen: (D) Fmoc-XF-Phe-DAP derivatives **2F**, **3F**, and **4F**; (E) Fmoc-XCl-Phe-DAP derivatives **2Cl**, **3Cl**, and **4Cl**; (F) Fmoc-XBr-Phe-DAP derivatives **2Br**, **3Br**, and **4Br**.

Table 2. Storage (G′) and loss (G″) moduli for hydrogels of Fmoc-X-Phe-DAP derivatives **2X–4X** reported as the average from three frequency sweeps. Error is reported as the standard deviation about the mean value.

Gelator	G′ (Pa)	G″ (Pa)
2F	21 ± 2	3.3 ± 0.2
2Cl	42 ± 3	8.6 ± 1.5
2Br	305 ± 31	42 ± 7
3F	1287 ± 51	214 ± 8
3Cl	1366 ± 4	131 ± 8
3Br	363 ± 48	36 ± 7
4F	1289 ± 110	121 ± 11
4Cl	78 ± 4	11 ± 1
4Br	573 ± 81	86 ± 7

The same data were also plotted in groups based on halogen identity to ascertain any further effects that each halogen had on the resulting hydrogel viscoelastic moduli (**Figure 3D–F**). For fluorinated hydrogels, *meta* (**3F**) and *para* (**4F**) substitution of the phenyl ring resulted in very similar G′ values, while *ortho* (**2F**) substitution resulted in the formation of a very weak hydrogel as discussed earlier (**Figure 3D**). Both the *ortho*-chlorinated (**2Cl**) and *para*-chlorinated (**4Cl**) derivatives formed very weak hydrogels as well, while *meta*-chlorinated hydrogels (**3Cl**) exhibited similar moduli to *meta*-fluorinated hydrogels (**3F**) (**Figure 3B** and **3E**). The most striking observation is the close moduli clustering of hydrogels composed of brominated gelators **2Br**, **3Br**, and **4Br**, when compared to the wider distribution of moduli of fluorinated and chlorinated hydrogels (**Figure 3F**). Network interactions facilitated by the presence of bromine in the phenyl side chain evidently dominate other effects in these samples to provide a relatively consistent

network strength regardless of the ring substitution pattern or observed assembly morphology. Halogen identity and position as well as the assembly morphology influence the hydrogel network viscoelasticity in self-assembled Fmoc-X-Phe-DAP derivatives. However, there are no obvious trends in this data, illustrating the complex relationship between the chemical structure of supramolecular gelators, the morphology of the resulting assemblies, and the emergent properties that arise from these networks.

Discussion. These data demonstrate how subtle, single-atom changes in the chemical structure of Fmoc-Phe-DAP based gelators dramatically affects the self-assembly and emergent material properties of these derivatives in an unpredictable manner. To attempt to rationalize the emergent supramolecular behavior of Fmoc-X-Phe-DAP gelators, it is instructive to consider prior reports of similar systems. First, we can compare these results to the patterns observed in self-assembly and gelation of previously reported Fmoc-X-Phe derivatives.[46] The Fmoc-X-Phe derivatives presented more obvious trends in the viscoelastic storage and loss moduli than was observed for the cationic Fmoc-X-Phe-DAP systems discussed herein. The viscoelastic moduli for Fmoc-X-Phe derivatives decreased with halogen electronegativity from F > Cl > Br when comparing derivatives with identical halogen substitution position on the phenyl side chain. Additionally, the moduli for Fmoc-X-Phe hydrogels generally decreased as the substitution pattern changed from *meta* > *ortho* > *para*. In contrast, the cationic Fmoc-X-Phe-DAP derivative hydrogels reported herein presented no obvious trend in viscoelastic moduli related to the halogen identity at each position. The *ortho*-substituted Fmoc-2X-Phe-DAP hydrogels produced the lowest viscoelastic moduli of the positional variants with no clear trend emerging in the case of *meta*- or *para*-substituted hydrogels. One possible explanation for these findings is the significant morphological

differences between these two gelator systems. Fmoc-X-Phe derivatives with unmodified C-terminal carboxyl groups self-assembled into similar fibrils regardless of side-chain halogen identity or position. However, the cationic Fmoc-X-Phe-DAP class of gelators assemble to form a more diverse set of polymorphic assembly morphologies, ranging from fibrils to nanoribbons to nanotubes, that may either enhance or destabilize overall network interactions between the fibrils/nanoribbons/nanotubes present in a particular sample.

Additionally, we can consider reports of structural data available for similar systems to gain further insight into the potential packing interactions of the Fmoc-X-Phe-DAP systems. Since many Fmoc-Phe derivatives are prone to gelation through supramolecular assembly, they are often difficult to crystallize. There are examples of Fmoc-Phe derivatives that undergo serendipitous hierarchical assembly from hydrogel fibrils to crystals, which has enabled high-resolution x-ray diffraction analysis to define the packing structure of these derivatives.[27,38,41,52] These crystal structures have been used to infer possible packing architectures in the initially formed hydrogel fibrils, although it is debatable how similar these structures are to the packing architecture in the hydrogel state.[27,41,53-55] However, in the absence of readily available techniques to obtain high-resolution data of the native hydrogel packing architecture, crystal data is suggestive of key interactions that may influence self-assembly.

We and others have been able to obtain crystal packing data for Fmoc-Phe and a several closely related structural derivatives with substitutions at the phenyl side chain.[27,38,52,56-58] While Fmoc-Phe derivatives differ at the C-terminus from the Fmoc-Phe-DAP gelators described herein, they may provide clues that help explain the halogen substituent effects exhibited by Fmoc-Phe-DAP derivatives. Packing along the one-dimensional stack unit of Fmoc-Phe crystals is facilitated by backbone H-bonds between the amide NH and Fmoc carbonyl oxygen of neighboring

molecules, as well as offset face-to-face fluorenyl-fluorenyl and phenyl-phenyl π-π interactions (**Figure 4A** and **4B**).[27,52,56] The orientation of side chain phenyl-phenyl stacking has given some insight into how substitution of the phenyl ring perturbs the ring electronics, which in turn influences the energetics of phenyl-phenyl aromatic and dipole-dipole interactions in assemblies (**Figure 4C** and **4D**).[38] For example, *para* substitution of the phenyl side chain with electron withdrawing groups introduces a favorable dipolar interaction between the electronegative atom in the *para* substituent and a neighboring partial positive H atom, as exemplified by side chain packing data retrieved from crystals of Fmoc-4-NO_2-Phe (**Figure 4D**).[38,52] It is theorized that this interaction could also stabilize self-assembly into the hydrogel state, since Fmoc-Phe derivatives with electron-deficient substituents at the para position had enhanced gelation rates compared to those with electron-rich substituents.[38] Additionally, another interaction is found between the partially positive H atom *ortho* to the substituent and the partially negative C atom on the neighboring ring that is *meta* to the substituent (**Figure 4C** and **4D**). If a similar offset parallel phenyl ring arrangement is present in the Fmoc-Phe-DAP class of gelators, these stabilizing interactions may be greatly perturbed by addition of electronegative halogens to the different positions of the ring.

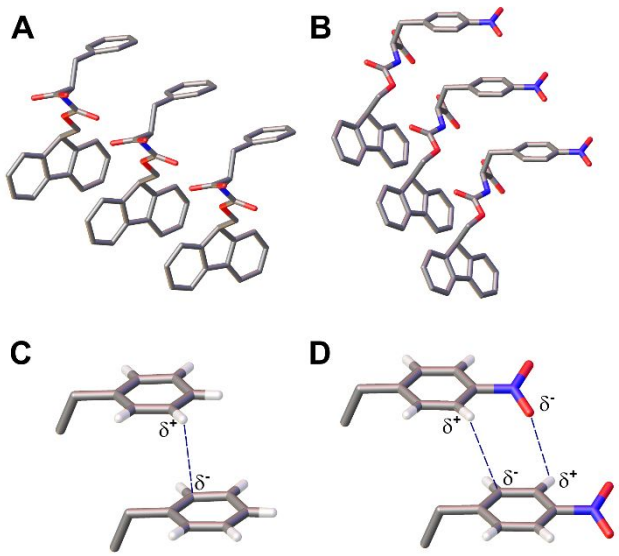

Figure 4. (A) Molecular packing arrangement of Fmoc-Phe in the crystalline state (retrieved from the Cambridge Crystallographic Data Centre, identifier VERXUO).[56] (B) Molecular packing arrangement of Fmoc-4-NO_2-Phe in the crystalline state (retrieved from the Cambridge Crystallographic Data Centre, identifier PEBTAV).[52] (C) Partial packing arrangement of the side-chain phenyl rings of Fmoc-Phe. (D) Partial packing arrangement of the side-chain phenyl rings of Fmoc-4-NO_2-Phe. Key dipolar interactions are highlighted between offset parallel side-chain phenyl rings of neighboring molecules.

Additional data that may be considered is the characterization of *para*-halogenated Fmoc-Phe derivatives by Pizzi *et al*.[57] It was found that halogen bonding interactions between the halogen atom and neighboring Fmoc aromatic ring systems were present in crystal structures of Fmoc-4Br-Phe and Fmoc-4I-Phe, but absent in structures of Fmoc-4F-Phe and Fmoc-4Cl-Phe. In fact, while Fmoc-4F-Phe and Fmoc-4Cl-Phe crystallized in an overall packing arrangement similar to unmodified Fmoc-Phe, the presence of halogen bonding in iodinated and brominated derivatives reinforced a different hexagonal packing architecture between the 1D stacks of molecules,

highlighting the strength of this interaction. It could be reasonable to believe that such halogen bonding interactions may also be present in our brominated Fmoc-X-Phe-DAP derivatives. Such an interaction could be the dominant force responsible for the similar viscoelastic moduli shared by the brominated derivatives. It is important to remember that the insights we stand to gain from all the aforementioned structural studies are greatly limited without further high-resolution characterization of these materials using emerging structural techniques that are beyond the scope of this work. Additional structural analyses using techniques, such as cryo-EM, that can provide high resolution models of Fmoc-Phe-DAP derivative supramolecular packing will enable explanations of the fascinating empirical results reported herein.

Conclusion

Herein, we have demonstrated the significant impact that single-atom substitutions to a LMW gelator scaffold can have on self-assembly and emergent properties of the assembly network. Self-assembly of Fmoc-X-Phe-DAP derivatives proved to be sensitive to monohalogenation at the phenyl side chain as evidenced by the variable formation of fibrils, nanoribbons, and nanotubes as a function of halogen identity and substitution pattern. The identity and position of the halogen substituent also influenced gelation potential and subsequent hydrogel viscoelastic moduli in ways that are not neatly summarized in trends, underscoring the complexities of these supramolecular systems. This work motivates further research into the relationship between chemical gelator structure and emergent self-assembly and gelation behavior. Further research into these phenomena may include the use of emerging high-resolution structural techniques such as cryo-EM, as well as leveraging artificial intelligence and machine learning to bridge the gap in our understanding of the correlation between structure and supramolecular

outcomes. This will be of paramount importance to enable rational design of LMW gelators with specific emergent properties suitable for applications such as drug delivery, tissue engineering, and regenerative medicine.

Author Contributions

BLA and BLN were responsible for experimental design. BLA, SGM, and BRG performed all experiments. The manuscript was written and edited by BLA, SGM, BRG, and BLN.

Conflicts of Interest

There are no conflicts to declare.

Acknowledgements

This work was supported by the National Science Foundation (DMR-1148836), the National Heart, Lung, and Blood Institute of the National Institutes of Health (R01HL138538), the Department of Defense (US Army Medical Research Acquisition Activity, W81XWH-20-1-0112), and a University of Rochester University Research Award. BLA was supported by a University of Rochester Robert L. and Mary L. Sproull Fellowship, Elon Huntington Hooker Fellowship, and Agnes M. and George Messersmith Fellowship. SGM was supported by a University of Rochester Discover Grant for Undergraduate Summer Research (sponsored by the Schwartz Undergraduate Research Fund). This research was facilitated by the services provided by the University of Rochester Mass Spectrometry Resource Laboratory and NIH instrument grant (S10OD021486), and we thank Kevin Welle for his assistance. We gratefully acknowledge Karen

Bentley and the URMC Electron Microscope Shared Resource for their assistance in TEM imaging experiments.

References

1. Zhou, J.; Li, J.; Du, X.; Xu, B. Supramolecular biofunctional materials. *Biomaterials* **2017**, *129*, 1-27.
2. Lyu, Y.; Azevedo, H. S. Supramolecular Hydrogels for Protein Delivery in Tissue Engineering. *Molecules* **2021**, *26*, 873.
3. Du, X.; Zhou, J.; Shi, J.; Xu, B. Supramolecular Hydrogelators and Hydrogels: From Soft Matter to Molecular Biomaterials. *Chem. Rev.* **2015**, *115*, 13165-13307.
4. Li, J.; Xing, R.; Bai, S.; Yan, X. Recent advances of self-assembling peptide-based hydrogels for biomedical applications. *Soft Matter* **2019**, *15*, 1704-1715.
5. Hellmund, K. S.; Koksch, B. Self-Assembling Peptides as Extracellular Matrix Mimics to Influence Stem Cell's Fate. *Front. Chem.* **2019**, *7*, 172.
6. Wang, Y.; Zhang, W.; Gong, C.; Liu, B.; Li, Y.; Wang, L.; Su, Z.; Wei, G. Recent advances in the fabrication, functionalization, and bioapplications of peptide hydrogels. *Soft Matter* **2020**, *16*, 10029-10045.
7. Liu, C.; Zhang, Q.; Zhu, S.; Liu, H.; Chen, J. Preparation and applications of peptide-based injectable hydrogels. *RSC Adv.* **2019**, *9*, 28299-28311.
8. Wang, Q.; Jiang, N.; Fu, B.; Huang, F.; Liu, J. Self-assembling peptide-based nanodrug delivery systems. *Biomater. Sci.* **2019**, *7*, 4888-4911.

9. Lopez-Silva, T. L.; Schneider, J. P. From structure to application: Progress and opportunities in peptide materials development. *Curr. Opin. Chem. Biol.* **2021**, *64*, 131-144.

10. Sis, M. J.; Webber, M. J. Drug Delivery with Designed Peptide Assemblies. *Trends Pharmacol. Sci.* **2019**, *40*, 747-762.

11. Gelain, F.; Luo, Z.; Rioult, M.; Zhang, S. Self-assembling peptide scaffolds in the clinic. *npj Regener. Med.* **2021**, *6*, 9.

12. Caliari, S. R.; Burdick, J. A. A practical guide to hydrogels for cell culture. *Nat. Methods* **2016**, *13*, 405-414.

13. Das, A. K.; Gavel, P. K. Low molecular weight self-assembling peptide-based materials for cell culture, antimicrobial, anti-inflammatory, wound healing, anticancer, drug delivery, bioimaging and 3D bioprinting applications. *Soft Matter* **2020**, *16*, 10065-10095.

14. Dou, X.-Q.; Feng, C.-L. Amino Acids and Peptide-Based Supramolecular Hydrogels for Three-Dimensional Cell Culture. *Adv. Mater.* **2017**, *29*, 1604062.

15. Gupta, S.; Singh, I.; Sharma, A. K.; Kumar, P. Ultrashort Peptide Self-Assembly: Front-Runners to Transport Drug and Gene Cargos. *Front. Bioeng. Biotechnol.* **2020**, *8*, 504.

16. Pal, S.; Mehta, D.; Dasgupta, U.; Bajaj, A. Advances in engineering of low molecular weight hydrogels for chemotherapeutic applications. *Biomed. Mater.* **2021**, *16*, 024102.

17. Lim, J. Y. C.; Lin, Q.; Xue, K.; Loh, X. J. Recent advances in supramolecular hydrogels for biomedical applications. *Mater. Today Adv.* **2019**, *3*, 100021.

18. Chakraborty, P.; Gazit, E. Amino Acid Based Self-assembled Nanostructures: Complex Structures from Remarkably Simple Building Blocks. *ChemNanoMat* **2018**, *4*, 730-740.

19. Das, R.; Gayakvad, B.; Shinde, S. D.; Rani, J.; Jain, A.; Sahu, B. Ultrashort Peptides—A Glimpse into the Structural Modifications and Their Applications as Biomaterials. *ACS Appl. Bio Mater.* **2020**, *3*, 5474-5499.

20. Zurcher, D. M.; McNeil, A. J. Tools for Identifying Gelator Scaffolds and Solvents. *J. Org. Chem.* **2015**, *80*, 2473-2478.

21. Draper, E. R.; Adams, D. J. Controlling the Assembly and Properties of Low-Molecular-Weight Hydrogelators. *Langmuir* **2019**, *35*, 6506-6521.

22. Draper, E. R.; Adams, D. J. Low-Molecular-Weight Gels: The State of the Art. *Chem* **2017**, *3*, 390-410.

23. Mushnoori, S.; Schmidt, K.; Nanda, V.; Dutt, M. Designing phenylalanine-based hybrid biological materials: controlling morphology via molecular composition. *Org. Biomol. Chem.* **2018**, *16*, 2499-2507.

24. Murali, D. M.; Shanmugam, G. The aromaticity of the phenyl ring imparts thermal stability to a supramolecular hydrogel obtained from low molecular mass compound. *New J. Chem.* **2019**, *43*, 12396-12409.

25. Singh, V.; Snigdha, K.; Singh, C.; Sinha, N.; Thakur, A. K. Understanding the self-assembly of Fmoc–phenylalanine to hydrogel formation. *Soft Matter* **2015**, *11*, 5353-5364.

26. Tao, K.; Levin, A.; Adler-Abramovich, L.; Gazit, E. Fmoc-modified amino acids and short peptides: simple bio-inspired building blocks for the fabrication of functional materials. *Chem. Soc. Rev.* **2016**, *45*, 3935-3953.

27. Draper, E. R.; Morris, K. L.; Little, M. A.; Raeburn, J.; Colquhoun, C.; Cross, E. R.; McDonald, T. O.; Serpell, L. C.; Adams, D. J. Hydrogels formed from Fmoc amino acids. *CrystEngComm* **2015**, *17*, 8047-8057.

28. Liyanage, W.; Vats, K.; Rajbhandary, A.; Benoit, D. S. W.; Nilsson, B. L. Multicomponent dipeptide hydrogels as extracellular matrix-mimetic scaffolds for cell culture applications. *Chem. Commun.* **2015**, *51*, 11260-11263.

29. Garcia, A.; Lavendomme, R.; Kralj, S.; Kurbasic, M.; Bellotto, O.; Cringoli, M. C.; Semeraro, S.; Bandiera, A.; De Zorzi, R.; Marchesan, S. Self-assembly of an amino acid derivative into an antimicrobial hydrogel biomaterial. *Chem. Eur. J.* **2019**, *26*, 1880-1886.

30. Shi, J.; Gao, Y.; Yang, Z.; Xu, B. Exceptionally small supramolecular hydrogelators based on aromatic–aromatic interactions. *Beilstein J. Org. Chem.* **2011**, *7*, 167-172.

31. Zhang, Y.; Kuang, Y.; Gao, Y.; Xu, B. Versatile small-molecule motifs for self-assembly in water and the formation of biofunctional supramolecular hydrogels. *Langmuir* **2011**, *27*, 529-537.

32. Mahler, A.; Reches, M.; Rechter, M.; Cohen, S.; Gazit, E. Rigid, Self-Assembled Hydrogel Composed of a Modified Aromatic Dipeptide. *Adv. Mater.* **2006**, *18*, 1365-1370.

33. Jayawarna, V.; Ali, M.; Jowitt, T. A.; Miller, A. F.; Saiani, A.; Gough, J. E.; Ulijn, R. V. Nanostructured Hydrogels for Three-Dimensional Cell Culture Through Self-Assembly of Fluorenylmethoxycarbonyl–Dipeptides. *Adv. Mater.* **2006**, *18*, 611-614.

34. Martin, A. D.; Robinson, A. B.; Thordarson, P. Biocompatible small peptide super-hydrogelators bearing carbazole functionalities. *J. Mater. Chem. B* **2015**, *3*, 2277-2280.

35. Martin, A. D.; Robinson, A. B.; Mason, A. F.; Wojciechowski, J. P.; Thordarson, P. Exceptionally strong hydrogels through self-assembly of an indole-capped dipeptide. *Chem. Commun.* **2014**, *50*, 15541-15544.

36. Das, T.; Haring, M.; Haldar, D.; Díaz Díaz, D. Phenylalanine and derivatives as versatile low-molecular-weight gelators: design, structure and tailored function. *Biomater. Sci.* **2018**, *6*, 38-59.

37. Quigley, E.; Johnson, J.; Liyanage, W.; Nilsson, B. L. Impact of gelation method on thixotropic properties of phenylalanine-derived supramolecular hydrogels. *Soft Matter* **2020**, *16*, 10158-10168.

38. Liyanage, W.; Nilsson, B. L. Substituent Effects on the Self-Assembly/Coassembly and Hydrogelation of Phenylalanine Derivatives. *Langmuir* **2016**, *32*, 787-799.

39. Aviv, M.; Cohen-Gerassi, D.; Orr, A. A.; Misra, R.; Arnon, Z. A.; Shimon, L. J. W.; Shacham-Diamand, Y.; Tamamis, P.; Adler-Abramovich, L. Modification of a Single Atom Affects the Physical Properties of Double Fluorinated Fmoc-Phe Derivatives. *Int. J. Mol. Sci.* **2021**, *22*, 9634.

40. Scarel, E.; Bellotto, O.; Rozhin, P.; Kralj, S.; Tortora, M.; Vargiu, A. V.; De Zorzi, R.; Rossi, B.; Marchesan, S. Single-atom substitution enables supramolecular diversity from dipeptide building blocks. *Soft Matter* **2022**, *18*, 2129-2136.

41. Fichman, G.; Guterman, T.; Damron, J.; Adler-Abramovich, L.; Schmidt, J.; Kesselman, E.; Shimon, L. J. W.; Ramamoorthy, A.; Talmon, Y.; Gazit, E. Spontaneous structural transition and crystal formation in minimal supramolecular polymer model. *Sci. Adv.* **2016**, *2*, e1500827.

42. Abraham, B. L.; Liyanage, W.; Nilsson, B. L. Strategy to Identify Improved N-Terminal Modifications for Supramolecular Phenylalanine-Derived Hydrogelators. *Langmuir* **2019**, *35*, 14939-14948.

43. Reddy, A.; Sharma, A.; Srivastava, A. Optically Transparent Hydrogels from an Auxin–Amino-Acid Conjugate Super Hydrogelator and its Interactions with an Entrapped Dye. *Chem. Eur. J.* **2012**, *18*, 7575-7581.

44. Nanda, J.; Biswas, A.; Banerjee, A. Single amino acid based thixotropic hydrogel formation and pH-dependent morphological change of gel nanofibers. *Soft Matter* **2013**, *9*, 4198-4208.

45. Ryan, D. M.; Anderson, S. B.; Senguen, F. T.; Youngman, R. E.; Nilsson, B. L. Self-assembly and hydrogelation promoted by F5-phenylalanine. *Soft Matter* **2010**, *6*, 475-479.

46. Ryan, D. M.; Anderson, S. B.; Nilsson, B. L. The influence of side-chain halogenation on the self-assembly and hydrogelation of Fmoc-phenylalanine derivatives. *Soft Matter* **2010**, *6*, 3220-3231.

47. Rajbhandary, A.; Raymond, D. M.; Nilsson, B. L. Self-Assembly, Hydrogelation, and Nanotube Formation by Cation-Modified Phenylalanine Derivatives. *Langmuir* **2017**, *33*, 5803-5813.

48. Raymond, D. M.; Abraham, B. L.; Fujita, T.; Watrous, M. J.; Toriki, E. S.; Takano, T.; Nilsson, B. L. Low-Molecular-Weight Supramolecular Hydrogels for Sustained and Localized in Vivo Drug Delivery. *ACS Appl. Bio Mater.* **2019**, *2*, 2116-2124.

49. Abraham, B. L.; Toriki, E. S.; Tucker, N. D. J.; Nilsson, B. L. Electrostatic interactions regulate the release of small molecules from supramolecular hydrogels. *J. Mater. Chem. B* **2020**, *8*, 6366-6377.

50. Ewoldt, R. H.; Johnston, M. T.; Caretta, L. M., Experimental Challenges of Shear Rheology: How to Avoid Bad Data. In *Complex Fluids in Biological Systems: Experiment,*

Theory, and Computation, Spagnolie, S. E., Ed. Springer: New York, NY, 2015; pp 207-241.

51. Dawn, A.; Kumari, H. Low Molecular Weight Supramolecular Gels Under Shear: Rheology as the Tool for Elucidating Structure–Function Correlation. *Chem. Eur. J.* **2017**, *24*, 762-776.

52. Liyanage, W.; Brennessel, W. W.; Nilsson, B. L. Spontaneous Transition of Self-assembled Hydrogel Fibrils into Crystalline Microtubes Enables a Rational Strategy To Stabilize the Hydrogel State. *Langmuir* **2015**, *31*, 9933-9942.

53. Dudukovic, N. A.; Hudson, B. C.; Paravastu, A. K.; Zukoski, C. F. Self-assembly pathways and polymorphism in peptide-based nanostructures. *Nanoscale* **2018**, *10*, 1508-1516.

54. Houton, K. A.; Morris, K. L.; Chen, L.; Schmidtmann, M.; Jones, J. T. A.; Serpell, L. C.; Lloyd, G. O.; Adams, D. J. On Crystal versus Fiber Formation in Dipeptide Hydrogelator Systems. *Langmuir* **2012**, *28*, 9797-9806.

55. Adams, D. J.; Morris, K.; Chen, L.; Serpell, L. C.; Bacsa, J.; Day, G. M. The delicate balance between gelation and crystallisation: structural and computational investigations. *Soft Matter* **2010**, *6*, 4144-4156.

56. Rajbhandary, A.; Brennessel, W. W.; Nilsson, B. L. Comparison of the Self-Assembly Behavior of Fmoc-Phenylalanine and Corresponding Peptoid Derivatives. *Cryst. Growth Des.* **2018**, *18*, 623-632.

57. Pizzi, A.; Lascialfari, L.; Demitri, N.; Bertolani, A.; Maiolo, D.; Carretti, E.; Metrangolo, P. Halogen bonding modulates hydrogel formation from Fmoc amino acids. *CrystEngComm* **2017**, *19*, 1870-1874.

58. Cohen-Gerassi, D.; Arnon, Z. A.; Guterman, T.; Levin, A.; Ghosh, M.; Aviv, M.; Levy, D.; Knowles, T. P. J.; Shacham-Diamand, Y.; Adler-Abramovich, L. Phase Transition and Crystallization Kinetics of a Supramolecular System in a Microfluidic Platform. *Chem. Mater.* **2020**, *32*, 8342-8349.